Analyst

PAPER

View Article Online
View Journal | View Issue

Cite this: *Analyst*, 2025, **150**, 2837

Surface charge regulation mediates anomalous ion transport in silica nanochannels

Kaushik K. Rangharajan and Shaurya Prakash *

A hybrid microfluidic–nanofluidic device was evaluated for the transport of a variety of ions with the purpose of enhancing the understanding of surface charge regulation for electrokinetic transport within silica nanochannels. A bank of three nanochannels at 16 nm depth connected two microfluidic channels that acted as fluid and electrolyte reservoirs for the experimental and modeling studies reported in this work. Surface charge regulation was noted to be dependent on the size of the hydrated cation, the type of anion, and the electrolyte concentration for the negatively charged silica nanochannels, with anomalous transport being observed. The results reported here provide new insight into the impact of surface charge regulation as a function of ion type and electrolyte concentration within nanochannels and subsequently raise the possibility of tuning electrolyte solution composition to manipulate surface charge and subsequent electroosmotic flow within nanochannels.

Received 21st February 2025,
Accepted 8th May 2025

DOI: 10.1039/d5an00198f

rsc.li/analyst

Introduction

Nanoscale conduits like nanochannels, nanopores, and nanotubes present important interfaces in biological[1,2] and engineered systems[3] for water desalination,[4,5] energy generation,[6–10] biosensors,[11] or fluidic analogues of solid-state electronics.[10,12–16] Essential for the viability of all these applications is a clear, complete, and mechanistic understanding of fundamental nanoconduit-surface–ion–water interactions, which vary significantly from bulk flows[17,18] due to high surface area to volume ratios, with the nanoconduit surface charge having been identified as an essential variable impacting electrokinetic nanoscale flows.[19,20]

Modulation of surface charge within nanoscale conduits is particularly important when the electrokinetic radius,[21,22] *i.e.*, the ratio of nanoconduit size to electric double layer (EDL) thickness is $O(1)$, as at these scales ionic selectivity and transport are governed by the surface charge. In this context, recent reports have highlighted the critical role of the phenomenon of surface charge regulation,[23,24] *i.e.*, the change in surface charge due to ion or solute interactions with nanoconduit walls.[25] Charge regulation has been shown to influence surface potentials within a nanofluidic device governed by characteristic length scales and geometries, the separation distance of electric double layers, the solution composition, or the applied voltages.[26] Surface charge regulation[27,28] has also been associated with reports of anomalous mole fraction effects due to nanoscale conduits presenting a lower ionic conductance with ion mixtures in solution in comparison with the same concentration of either ionic species by itself.[27] The effect of charge regulation is significantly enhanced when working with dilute electrolyte solutions as the EDL occupies a significant fraction of nanoconduits. Moreover, recent work has also evaluated the regulation of surface charge leading to reversal of the native surface charge polarity due to excessive charge screening.[29]

Notably, the interaction of ions in solution with surface charges has been a topic of intense study for many years with the screening of surface charge being known to be highly dependent on the chemical structure of the entire solution.[25] Theoretically, these investigations have largely focussed on the use of mean field theories such as the Poisson–Boltzmann equation; however, neither these theories work well in multivalent systems with strong ion–ion correlations, nor do these theories account for variations in ion and water densities near physical surfaces, discrete ionic and molecular sizes, and hydration of solvated ions.[20,28] Therefore, advanced methods such as molecular dynamics simulations have been used to elucidate molecular details of ion–surface interactions.[29]

Previous studies have also reported surface charge regulation, including the phenomenon of charge inversion, as a key mediator of ion transport within nanoconduits.[20,23,29–31] Yet, a key knowledge gap remains – there is a paucity of experimental data demonstrating charge regulation for a variety of cations and anions. Nearly all reported data remain limited to K^+ with some emerging reports on Na^+, Ca^{2+}, and Mg^{2+} as other cations of interest.[23,24,32,33] It is worth noting that there are no reports evaluating the effect of different anions in solution beyond the monovalent anion Cl^-.

Department of Mechanical and Aerospace Engineering, The Ohio State University, 201 W. 19th Avenue, Columbus, OH 43210, USA. E-mail: prakash.31@osu.edu

In this study, we report the experimental data on the transport of a broad array of both cations (Na^+, K^+, Ca^{2+}, Mg^{2+}, and Ba^{2+}) and anions (Cl^- and SO_4^{2-}) through a parametric evaluation of valence and ion size (including hydrated ion radii) in slit-like (16 nm deep) silica nanochannels. Given the purpose of this work, that is, to report experimental data for ion transport in nanochannels, both cations and anions were chosen to reflect comparative analyses with known ions. Therefore, K^+ and Cl^- present validation to existing data. Mg^{2+} and Ca^{2+} complement the largely numerical work for additional ions, with new trends being reported that enhance some of the literature on divalent ion transport. Ba^{2+} is an emerging ion for a variety of applications such as water treatment of difficult-to-treat waters. Finally, the anion SO_4^{2-} was chosen as a common divalent anion that complements the presence of chloride in applications such as water treatment.[34] Our evaluation shows deviations from trends expected from the current state-of-the-art suggesting that surface charge regulation can lead to anomalous ion transport within nanochannels.

Methods

Nanofluidic device fabrication

The nanofluidic device uses two microfluidic channels (8 μm (H) × 50 μm (W) × 3 cm (L)) as fluidic reservoirs to connect a bank of three ultra-low aspect ratio (ULAR) nanochannels, 16 nm deep (30 μm (W) × 2.5 mm (L)). The fabrication process has been reported previously.[35,36] Briefly, the micro- and nanofluidic channel network was patterned on a borosilicate glass substrate using standard UV lithography followed by wet etching using hydrofluoric acid (HF; Sigma-Aldrich). The top glass cover with holes drilled for fluidic access and the bottom glass slide comprising the etched channels were bonded using calcium-assisted glass bonding.[37] The fabrication results in a hybrid microfluidic–nanofluidic device with fluorescence verification of flow in the nanochannels as shown in Fig. 1.

Device operation

The microfluidic and nanofluidic channels were initially filled with various salt solutions prepared in de-ionized water to yield concentrations ranging from 0.001 to 10 mM. All salts ($CaCl_2$, $BaCl_2$, $MgCl_2$, and $CaSO_4$) were purchased from Sigma-Aldrich and used without modification. The pH of all solutions was monitored and maintained at 7.2 ± 0.2 with experiments conducted at room temperature. All nanochannel conductance measurements were conducted using methods previously reported and in an earth-grounded Faraday cage to minimize electrical interference.[23,38] Briefly, the device testing setup included a power supply (Keithley 3390 function generator) used to apply a streamwise-axial (V_a) potential with V_a = 2 V. Current (I) through the nanochannels was monitored using a Keithley 6485 picoammeter. Devices were tested at each respective concentration to measure the intrinsic nanochannel conductance. Dedicated devices for each type of electrolyte were used to avoid contamination. Each device was initially tested with deionized (DI) water (18 MΩ, 10^{-7} M salt) to provide the same baseline for comparison between devices. Only devices with an initial DI water conductance within 0.15 ± 0.1 nS were used for comparison of results across devices as a function of ion type. The reported intrinsic DI-water conductance in the channels is similar to that reported in previous work[39] and confirms the valid operation of our devices.

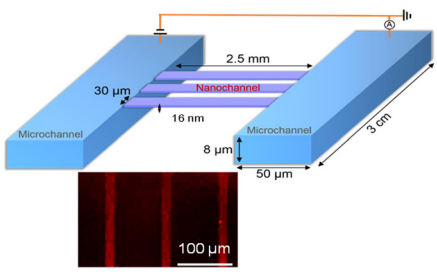

Fig. 1 Schematic showing the layout of the microfluidic–nanofluidic device. The inset shows a fluorescence image for 0.1 mM rhodamine in DI water to confirm that the nanochannels are viable for conductance measurements. The fluorescence image contrast was enhanced to clearly show the nanochannel operation.

Numerical modelling

The hybrid microfluidic–nanofluidic device can be modelled using well-known governing equations that have also been reported previously.[13,40] Briefly, the nanochannel was modelled as a symmetric nanochannel with a total depth of 16 nm. The primary experimentally measured parameter is the electric current, arising from the flux of ions $\vec{J}_i$ as given by eqn (1).

$$\vec{J}_i = -D_i \nabla c_i - \varepsilon_i z_i F c_i \nabla \Phi + c_i \vec{u} \quad (1)$$

For a given species i, D_i is the diffusion coefficient, c_i is the concentration, ε_i is the ionic mobility, z_i is the ion valence, Φ is the potential, and $\vec{u}$ is the convective velocity. Ionic mobility is related to the diffusion coefficient as $\varepsilon_i = eD_i/k_bT$ where e is the elementary charge, k_b is the Boltzmann constant, and T is the absolute temperature.[41] The summation of the ionic flux across all the species and subsequently integrating over the cross-section area and multiplying with the Faraday constant (F) and valence of each species then provides the total ionic current, I, which is typically measured.[40] The steady-state flux continuity is given by

$$\nabla \cdot \vec{J}_i = 0. \quad (2)$$

The model assumed an incompressible, isothermal fluid with the viscosity, density, and electrical permittivity of water remaining constant. The inlet and exit concentrations of ionic species were assumed to be the same as those of the bulk, defined by the experimental conditions. No ionic flux normal to nanochannel or microchannel walls was permitted.[13] The equilibrium potential in the nanoscale conduit and the microchannel reservoirs is governed by the Poisson equation as follows:

$$\varepsilon_0 \varepsilon_w \nabla^2 \Phi = -\rho_s$$
$$\rho_s = F \sum_i z_i c_i \quad (3)$$

where ε_0 is the permittivity of free space, ε_w (= 80) is the permittivity of water, and ρ_s is the volumetric space charge density. A Dirichlet boundary condition was applied for the potential in the microchannel reservoirs such that the inlet reservoir potential is the same as the inlet axial potential from the experimental conditions. The bulk transport of water was subject to the following equations,

$$\nabla \cdot \vec{u} = 0$$
$$-\nabla p + \mu \nabla^2 \vec{u} - \rho_s \nabla \Phi = 0 \quad (4)$$

where μ is the dynamic viscosity of water at 293 K, p is the pressure, and $-\rho_s \nabla \Phi$ is the body force on the bulk fluid due to the space charge and the electric field. Therefore, conservation of mass and charge was applied, and the system was modelled using the Poisson–Nernst–Planck equations combined with the Navier–Stokes equations for fluid flow, as reported previously.[13,40] Lastly, the surface charge for the model was used as a fit parameter to obtain numerically the same conductance as measured experimentally.[23] Notably, as much literature exists on the modelling of these types of nanoscale transport, the readers are referred to well-established literature on these equations, including those in textbooks.[42,43] The equations were solved with COMSOL Multiphysics version 4.4. Solutions were verified for mesh independence, and the relative tolerance for convergence was set to 10^{-6} similar to previous work.[40]

Results and discussion

Context for results

Previous work on surface charge regulation has shown that at a particular electrolyte concentration, the surface charge polarity can change, *i.e.*, for a negative surface, adsorption of cations causes the surface charge polarity to become positive leading to a phenomenon referred to as charge inversion (CI). We begin our reporting through evaluation of important previous results as there remain significant discrepancies between reported results for silica surfaces for similar ions.[28,44] Towards the illustration of these discrepancies, a summary of key previous results is reported for both charge inversion and surface charge regulation in Fig. 2. It is worth noting that for a well-studied material like silica, there is no consensus on the surface charge or electrolyte concentration for charge inversion, despite testing under similar conditions by multiple researchers. For silica, much data are available on monovalent cations such as K^+ (Fig. 2A). Fig. 2 shows that the range of surface charge values reported remains broad; however, as shown in Fig. 2B and C, respectively, the discrepancy in the reported values of surface charge for divalent cations, such as those evaluated herein, Ca^{2+} and Mg^{2+}, is also significant while much less experimental data are available. Real-world systems in many applications such as water desalination or energy harvesting use complex mixtures of ions subject to nanoscale transport and the lack of available data continues to be a hindrance in the systematic design of new systems.

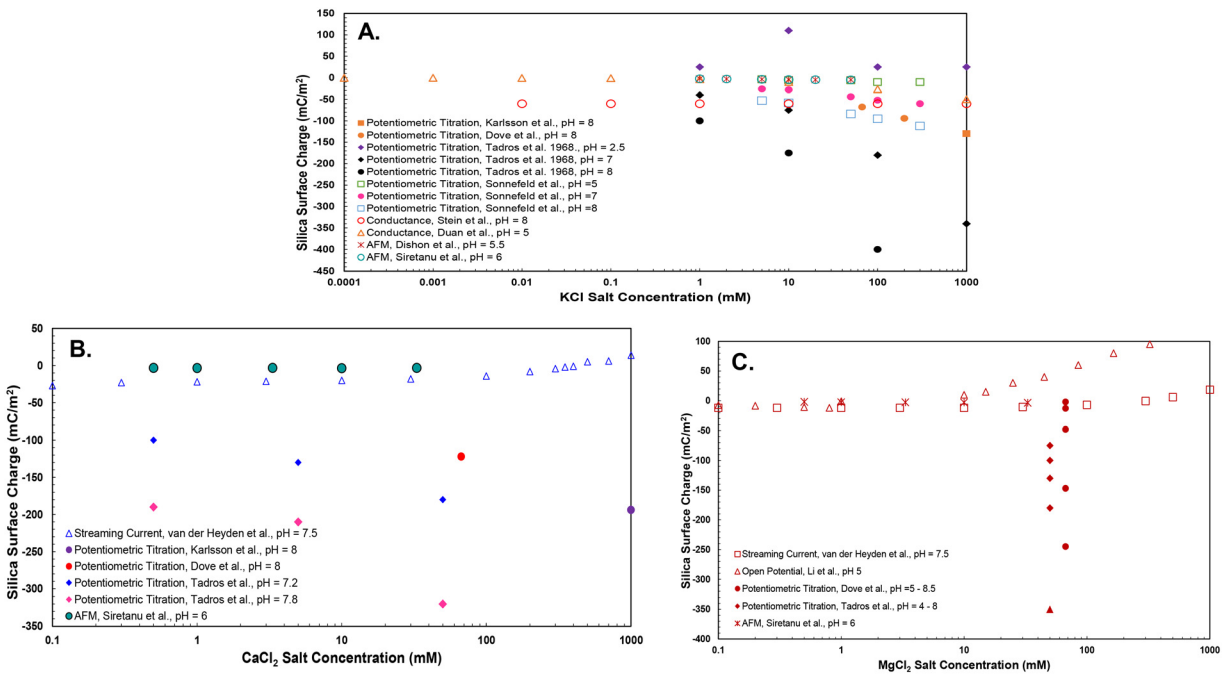

Fig. 2 Summary of some previously reported studies that shows the discrepancies in reporting of silica surface charge under similar conditions, with different electrolytes (A) KCl, (B) $CaCl_2$, and (C) $MgCl_2$. The different experimental methods are also noted. The figure also illustrates the relative paucity of data for divalent cations and other electrolytes beyond monovalent electrolytes.

Experimental evaluation of nanochannel conductance

Nanochannel transport data for electrokinetic flows are usually reported as nanochannel conductance (Fig. 3) to quantify the ion transport.[20] Such an approach has led to the classification of two main transport regimes, where the bulk transport governed regime (BTGR) at higher ionic strengths shows an ohmic response with increasing electrolyte concentration while in the surface charge governed regime (SCGR) the nanochannel conductance is independent of the electrolyte concentration, typically at dilute electrolyte concentrations.[19] To satisfy electroneutrality, the total space charge within the nanochannel volume must balance the total surface charge on the nanochannel walls. G_a is thus the summation of the SCGR and the BTGR conductance as shown in the equation below:[20,28]

$$G_a = G_{SCGR} + G_{BTGR} = \frac{2w\mu_+|\sigma|}{L} + \frac{Fwh}{L}\sum_{i=1}^{i=n}\mu_i z_i^2 c_i^{bulk} \quad (5)$$

where σ is the surface charge density (negative for glass) on the nanochannel walls, μ_i is the mobility of ionic species i, c_i^{bulk} is the bulk electrolyte concentration, and w, L, and h are the channel width, length, and height, respectively. The dominant conductance term in the equation, G_{SCGR} or G_{BTGR}, depends on the bulk electrolyte concentration. At the transition concentration where the transport regime shifts from surface-charge governed to bulk transport governed, both the conductances are similar.[13]

Notably, previous work has shown that the transition between the SCGR and the BTGR occurs approximately at 1 mM for silica nanochannels, regardless of the nanochannel size.[12,15,20] As shown in Fig. 3, the trends reported here agree with previous reports[12,15,20] meeting the two classifications of the SCGR and BTGR (dotted lines marked in Fig. 3 as visual guides). Fig. 3A shows that in the SCGR, Na^+ conductance was higher than K^+ conductance, within experimental error. However, in a new finding, the trend changes within the BTGR where K^+ conductance was observed to be greater than Na^+. In both cases, the anion was Cl^-.

Comparing ion sizes, for a bare ion, the size of $Na^+ < K^+$; however, when comparing hydrated ion sizes,[45] $K^+ < Na^+$. The change in measured nanochannel conductance is attributed to surface charge regulation and layering of ions due to differences in hydrated ion sizes.[31,46–51] A similar evaluation for comparing divalent ions Mg^{2+} and Ca^{2+} with Cl^- as the anion once again showed a similar trend, with Mg^{2+} conductance being higher than that with Ca^{2+} present within the nanochannels in the SCGR but the conductance of nanochannels with $CaCl_2$ as the electrolyte was noted to be higher in the BTGR (Fig. 3B). Once again, it is noted that for bare ions,[45] the size of $Mg^{2+} < Ca^{2+}$ but for hydrated ions, the size of $Ca^{2+} < Mg^{2+}$. Therefore, for these four cations, the larger hydrated cation dominates ion transport at higher concentrations and the smaller cation at lower concentrations, suggesting that in dilute solutions smaller cations may be more effective at screening surface charge.

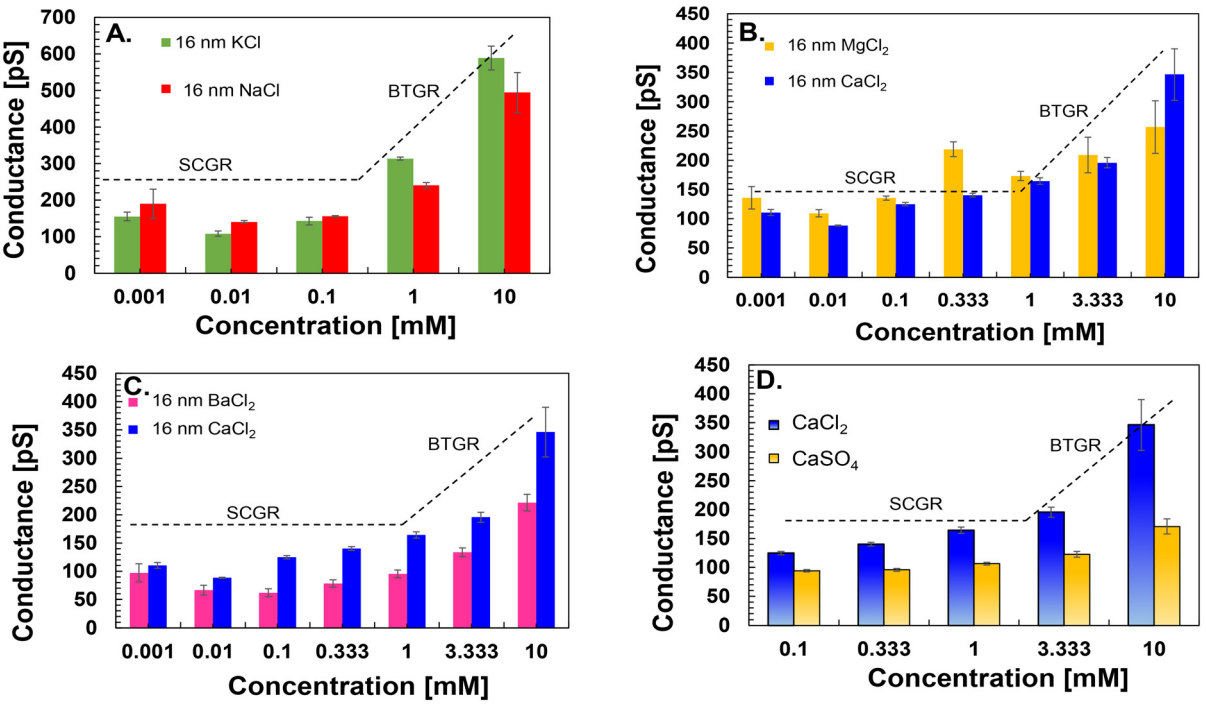

Fig. 3 Measured ionic conductance in 16 nm deep silica nanochannels. (A) Conductance comparison between monovalent cations Na^+ and K^+; (B) conductance comparison between divalent cations Mg^{2+} and Ca^{2+}; (C) conductance comparison between divalent cations Ba^{2+} and Ca^{2+}; and (D) conductance comparison for different anions while keeping the cation as Ca^{2+}. The dotted lines act as guides to the eye to show approximate regions for the SCGR and the BTGR.[19]

To further evaluate the effect of ion sizes mediating surface charge regulation, the conductance of nanochannels was measured with Ba^{2+} as the cation while keeping the anion fixed as Cl^-. Interestingly, the measured conductance for Ba^{2+} remains lower than that for Ca^{2+} across all tested concentrations (Fig. 3C) despite the fact that the size of a hydrated Ba^{2+} ion is smaller than that of a hydrated Ca^{2+} ion.[45] Therefore, Ba^{2+}-containing electrolyte solutions show anomalous transport with respect to Ca^{2+}-containing electrolyte solutions.

The nanochannels in the experiments conducted here present a negative surface charge. Since these silica walls were negatively charged, at dilute concentrations exclusions of the co-ions (*i.e.*, Cl^- and SO_4^{2-}) would be expected[52] and therefore the nanochannel conductance should remain invariant with respect to anions in the solution. Given the emerging importance of Ca^{2+} in nanofluidic applications,[4,53,54] we chose to test the validity of the anion independence by evaluating the electrokinetic transport of $CaSO_4$ through the silica nanochannels (Fig. 3D; yellow bars). As seen in Fig. 3D, the $CaSO_4$ containing nanochannels showed nearly concentration independent conductance, *i.e.*, the presence of SO_4^{2-} limits the transition from the SCGR to the BTGR. Moreover, in the entire concentration range tested, the measured conductance for $CaSO_4$-containing nanochannels was lower than that for those containing $CaCl_2$. Comparing anion sizes, as a bare ion the SO_4^{2-} ion is approximately 60% larger than a Cl^- ion, but is only *ca.* 14% larger in the hydrated state.[45] However, some previous results have noted that unless specific ion–nanochannel wall interactions are accounted for, perfect permselectivity may not occur.[40,52] Furthermore, the larger anion also exhibits a lower mobility and therefore the electrolyte transport presents a lower conductance.[24] Taken together, these observations explain the difference in the conductances of $CaCl_2$- and $CaSO_4$-containing nanochannels. Therefore, a new observation from these data arises despite the prevailing view that co-ions are excluded from nanochannels and do not contribute to ion transport. Here, we show that the type of anion and the respective hydrated ion sizes limit cationic transport and can extend the concentration regime for surface-charge governed transport.

To place these results in the context of previous work, it is worth noting that ion transport within nanoarchitectures may also be impacted by the entrance of ions from a larger reservoir to the nanochannel. Previously, the role of net charge in the EDL near a pore surface as the source of the observed surface conductance has been evaluated. The authors identified leakage of surface electric potential from the nanopore into the reservoir using molecular dynamics simulations. In another report for conical nanopores, electric fields at the nanopore entrance and exit regions induce large surface charges generating non-uniform EDLs with accumulation of electrolyte ions at the orifice. Presumably, the distribution of charges limits the transfer of ions through these nanopores. These, and similar previous studies, emphasize that asymmetry in the nanoscale conduit geometry or small aspect ratio nanoscale conduits may significantly be impacted by the reservoir-entrance effects, including a role of counterions.[50,51,55,56]

Surface charge estimation

Using the well-known governing equations described above, the nanochannel conductance was used to compute the silica charge as reported previously.[13] As the concentration of the bulk electrolyte increases and the transport of ions shifts from the SCGR to the BTGR, the surface charge for silica becomes progressively more positive indicating surface charge regulation due to likely cation adsorption. In this work, no charge inversion was observed. The lack of observed charge inversion agrees with previous reports that have identified significantly higher electrolyte concentrations for inversion than those evaluated here.[29,44] In contrast, another study reported that charge inversion for divalent cations can occur at lower concentrations.[28] Interestingly, the least negative surface charge was observed for Ba^{2+} as seen in Fig. 4A compared to Ca^{2+} and Mg^{2+} for the same anion (Fig. 4B and C, respectively). It is also worth noting that for the same anion Cl^-, Mg^{2+}, which presents the largest hydrated ion size among the three divalent cations, showed the largest range of surface charge (from ~ -0.2 C m^{-2} to -0.05 C m^{-2}) as the bulk electrolyte concentration was varied. In contrast, when comparing against a fixed anion, Ca^{2+} showed more charge regulation for the larger anion SO_4^{2-} (Fig. 4D). Therefore, for silica nanochannels, anions can also be used to modulate the cationic surface charge regulation in addition to known parameters such as pH or externally applied wall-electric potentials.[18]

Surface charge regulation impacts electroosmotic flow

It is well-known that the electroosmotic flow (EOF) displays ion and electrolyte composition-dependent behaviour, including for nanofluidic devices.[57] Using the surface charge density derived from the conductance measurements here, continuum

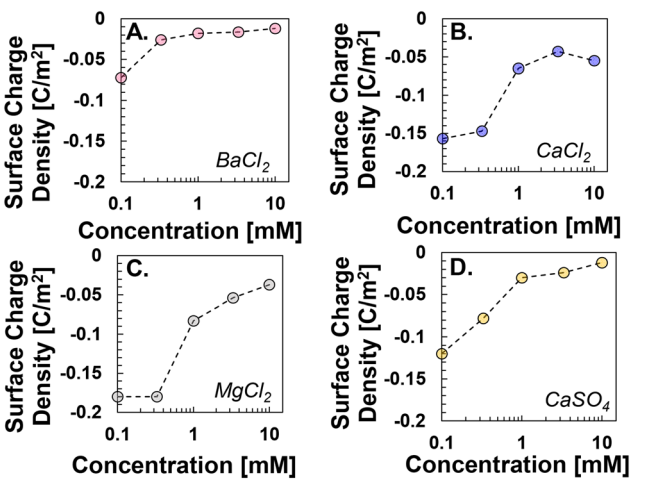

Fig. 4 Computed surface charge for silica nanochannels. (A) $BaCl_2$-containing channels; (B) $CaCl_2$-containing channels; (C) $MgCl_2$-containing channels; and (D) $CaSO_4$-containing channels. The dotted lines act as guides to the eye.

modelling based on well-established theoretical models was implemented and the resulting velocities are shown in Fig. 5. Notably, the nanochannel was modelled as a symmetric channel with the centerline in the nanochannel being the location of the highest velocity. A no-slip boundary condition was imposed at the nanochannel wall indicated by the 8 nm channel height with the model geometry shown in Fig. 5A.

Fig. 5B–D show the velocity profiles for each of the four electrolytes with divalent cations. As the bulk electrolyte concentration increased from 0.33 mM to 10 mM, the maximum EOF at the centerline was also noted to increase. Dilute solutions with electrolyte concentrations below 0.33 mM were not evaluated, as in the SCGR, the EOF velocity remains constant.[15] Interestingly, while at the lowest concentration of 0.33 mM $BaCl_2$ shows the highest EOF velocity of nearly 30 μm s^{-1}, at 10 mM, the computed EOF for $BaCl_2$ and that for $CaSO_4$ were nearly identical and both electrolytes showed a much smaller EOF than the other two electrolytes, $CaCl_2$ and $MgCl_2$. Moreover, as can be seen from Fig. 5B–D, the maximum EOF for $MgCl_2$ changes from *ca.* 5 μm s^{-1} to a highest EOF of *ca.* 70 μm s^{-1} at 3.33 mM and reduces to *ca.* 60 μm s^{-1} at 10 mM. On the other hand, $CaCl_2$ shows a near monotonic increase with the computed EOF rising from 10 μm s^{-1} at 0.33 mM to 70 μm s^{-1} at 10 mM.

Ion-transport based on standard electromigration theories suggests that the EOF velocities should scale inversely with the size of the cation. The Pauli radii of the divalent cations follow the trend $Mg^{2+} < Ca^{2+} < Ba^{2+}$. Therefore, the EOF is expected to follow the trend $Ba^{2+} < Ca^{2+} < Mg^{2+}$ with Cl^- as the anion. However, the calculated EOF that accounts for surface charge regulation shows a much more nuanced picture. Specifically, at the electrolyte concentration of 0.33 mM, the EOF trends follow the hydrated ion size trends (*i.e.*, $Ba^{2+} < Ca^{2+} < Mg^{2+}$ for EOFs being $Mg^{2+} < Ca^{2+} < Ba^{2+}$), reflecting that in the SCGR the wall charge regulation controls the EOF, as expected. However, when the anion was changed with $CaSO_4$ as the electrolyte, it was noted that the EOF of $CaCl_2 < CaSO_4$, suggesting that anions also play a role in surface charge regulation leading to unexpected changes in the EOF. When further exploring the nuances of the EOF in the transition region between the SCGR and the BTGR (*i.e.*, 1 mM and 3.33 mM), additional anomalous transport was observed. At 1 mM, the EOF followed the trend $MgCl_2 \approx CaCl_2 \leq CaSO_4 < BaCl_2$, while at 3.33 mM the trend once again shifted to $BaCl_2 < CaSO_4 < CaCl_2 \leq MgCl_2$. At 10 mM which falls within the BTGR, the EOF follows the trend $BaCl_2 < CaSO_4 < MgCl_2 < CaCl_2$.

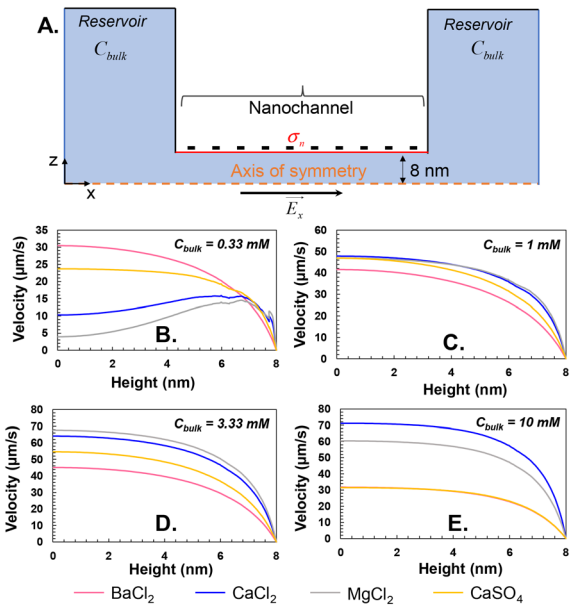

Fig. 5 Numerically calculated EOF for the silica channels. (A) Model geometry with the silica nanochannel modelled as a symmetric channel about the centerline. (B–E) EOF velocity profiles for the four electrolytes at four distinct concentrations as labelled on the plots.

The challenges with the use of PNP equations combined with Navier–Stokes equations in the absence of steric effects are worth noting, and the model presents validation of the device operation to add confidence in experimental data by showing the generally accepted trends for nanochannel conductance and EOF. Therefore, future work that accounts for steric effects with accurate hydration models for both the cationic and anionic species used in this primarily experimental report can likely elucidate the underlying mechanisms influencing the observed EOF trends.

Collectively, the change in EOF with ionic concentration with added dependence on the co-ion type is a new finding, especially for dilute electrolytes where the EDLs interact. To better understand the nuanced impact of charge regulation on the EOF, it is worth considering that in a recent modelling evaluation, the interplay between convection, surface-charge regulation, and slip length was evaluated for charged nanopores[58] to enable future design guides for operation of electrokinetically driven nanofluidic devices. Moreover, Li *et al.* showed that in channels at 85 nm, the EOF for KCl and $CaCl_2$ can be similar to charge regulation.[31] Clearly, both cation and anion type along with electrolyte concentration can be used to regulate surface charge and thereby enhance control over the EOF.

Summary and conclusions

In this study, a hybrid microfluidic–nanofluidic device was evaluated for the transport of a variety of ions with the purpose of enhancing the understanding of surface charge regulation and electrokinetic transport within silica nanochannels. Surface charge regulation was noted to be dependent on the size of the hydrated cation for the negatively charged silica nanochannels. Furthermore, when exploring size-dependent ion transport, anomalous transport of Ba^{2+} as a divalent cation was noted when compared against the trends observed for Mg^{2+} and Ca^{2+}. The size dependent ionic conductance trends were also verified for monovalent cations Na^+ and K^+. The surface charge regulation leads to the possibility of using an

electrolyte solution's composition and concentration to manipulate the surface charge and the subsequent electroosmotic flow within nanochannels.

Data availability

Data were acquired in the Microsystems and Nanosystems Laboratory at The Ohio State University and are archived as part of the dissertation of Dr Kaushik Rangharajan. The dissertation with supporting data is accessible through The Ohio State University Library System.

Conflicts of interest

The authors do not have any competing conflicts of interest.

Acknowledgements

The authors acknowledge the staff at Nanotech West Laboratories at The Ohio State University for assistance with equipment during fabrication and characterization of devices, Ohio Supercomputer for providing computational resources. The authors acknowledge partial financial support from the National Science Foundation (NSF) through grant CBET-1335946, the U.S. Department of Energy through grant DE-FE0024357, and the U.S. Department of Defense through grant CA210874.

References

1 A. Harsman, V. Kruger, P. Bartsch, A. Honigmann, O. Schmidt, S. Rao, C. Meisinger and R. Wagner, *J. Phys.: Condens. Matter*, 2010, **22**, 454102.
2 W. Wickner and R. Schekman, *Science*, 2005, **310**, 1452–1456.
3 S. Prakash and J. Yeom, *Nanofluidics and microfluidics: systems and applications*, Elsevier, Norwich, MA, 2014.
4 S. J. Kim, S. H. Ko, K. H. Kamg and J. Han, *Nat. Nanotechnol.*, 2010, **5**, 297–301.
5 M. A. Shannon, P. W. Bohn, M. Elimelech, J. G. Georgiadis, B. J. Marinas and A. M. Mayes, *Nature*, 2008, **452**, 301–310.
6 S. K. Mehta, P. Padhi, S. Wongwises and P. K. Mondal, *Microsyst. Technol.*, 2024, 1–10, DOI: **10.1007/s00542-024-05763-3**.
7 S. K. Mehta, P. Padhi, S. Wongwises and P. K. Mondal, *Langmuir*, 2024, **40**, 18750–18759.
8 S. K. Mehta, D. Deb, A. Nandy, A. Q. Shen and P. K. Mondal, *Phys. Chem. Chem. Phys.*, 2024, **26**, 20550–20561.
9 S. K. Mehta, A. Ghosh, P. K. Mondal and S. Wongwises, *Phys. Fluids*, 2024, **36**, 023101.
10 D. Pandey, P. K. Mondal and S. Wongwises, *Soft Matter*, 2023, **19**, 1152–1163.
11 M. A. Bakshloo, J. J. Kasianowicz, M. Pastoria-Gallego, J. Mathe, R. Daniel, F. Piguet and A. Oukhaled, *J. Am. Chem. Soc.*, 2022, **144**, 2716–2725.
12 M. Fuest, C. Boone, K. K. Rangharajan, A. T. Conlisk and S. Prakash, *Nano Lett.*, 2015, **15**, 2365–2371.
13 W. Guan, R. Fan and M. A. Reed, *Nat. Commun.*, 2011, **2**, 506.
14 R. Karnik, K. Castelino and A. Majumdar, *Appl. Phys. Lett.*, 2006, **88**, 123114.
15 R. Karnik, R. Fan, M. Yue, D. Li, P. Yang and A. Majumdar, *Nano Lett.*, 2005, **5**, 943–948.
16 D. Pandey and P. K. Mondal, *Phys. Fluids*, 2023, **35**, 082002.
17 C.-M. Kim, E. Yang, R. Karnik, R. W. Field, R. G. Fane, P. Wang and I. S. Kim, *Chem. Eng. J.*, 2025, **505**, 158366.
18 J. P. de Souza, C.-M. Chow, R. Karnik and M. Z. Bazant, *Phys. Rev. E*, 2021, **104**, 04482.
19 S. Prakash and A. T. Conlisk, *Lab Chip*, 2016, **16**, 3855–3865.
20 R. B. Schoch, J. Han and P. Renaud, *Rev. Mod. Phys.*, 2008, **80**, 839–883.
21 D. Burgreen and F. R. Nakache, *J. Phys. Chem.*, 1964, **68**, 1084–1091.
22 C. L. Rice and R. Whitehead, *J. Phys. Chem.*, 1965, **69**, 4017–4024.
23 M. Fuest, K. K. Rangharajan, C. Boone, A. T. Conlisk and S. Prakash, *Anal. Chem.*, 2017, **89**, 1593–1601.
24 P. Ramirez, J. A. Manzanares, J. Cervera, V. Gomez, M. Ali, S. Nasir, W. Ensinger and S. Mafe, *Electrochim. Acta*, 2019, **325**, 134914.
25 J. Lyklema, *Colloids Surf., A*, 2006, **291**, 3–12.
26 C.-Y. Lin, T. E. Acar, J. W. Polster, K. Lin, J.-P. Hsu and Z. S. Siwy, *ACS Nano*, 2019, **13**, 9868–9879.
27 D. Gillespie, D. Boda, Y. He, P. Apel and Z. S. Siwy, *Biophys. J.*, 2008, **95**, 608–619.
28 S. X. Li, W. Guan, B. Weiner and M. A. Reed, *Nano Lett.*, 2015, **15**, 5046–5051.
29 A. Rojano, D. Becerra, J. H. Walther, S. Prakash and H. A. Zambrano, *Phys. Fluids*, 2024, **36**, 102025.
30 S. H. Behrens and M. Borkovec, *J. Chem. Phys.*, 1999, **111**, 382–385.
31 J. Li, R. Peng and D. Li, *Anal. Chim. Acta*, 2019, **1059**, 68–79.
32 Y. He, D. Gillespie, D. Boda, I. Vlassiouk, R. S. Eisenberg and Z. S. Siwy, *J. Am. Chem. Soc.*, 2009, **131**, 5194–5202.
33 T. Jain, B. C. Rasera, R. J. S. Guerrero, M. S. H. Boutilier, S. C. O'Hern, J. C. Idrobo and R. Karnik, *Nat. Nanotechnol.*, 2015, **10**, 1053–1057.
34 K. K. Rangharajan, P. M. Sundaram, A. T. Conlisk and S. Prakash, *Analyst*, 2018, **143**, 4256–4266.
35 M. Fuest, K. K. Rangharajan, C. Boone, A. T. Conlisk and S. Prakash, *Anal. Chem.*, 2017, **89**, 1593–1601.
36 M. Pinti, T. Kambham, B. Wang and S. Prakash, *J. Nanotechnol. Eng. Med.*, 2013, **4**, 020905.
37 P. B. Allen and D. T. Chiu, *Anal. Chem.*, 2008, **80**, 7153–7157.

38 K. K. Rangharajan and S. Prakash, *Analyst*, 2022, **147**, 3817–3821.
39 C. Duan and A. Majumdar, *Nat. Nanotechnol.*, 2010, **5**, 848–852.
40 K. K. Rangharajan, M. Fuest, A. T. Conlisk and S. Prakash, *Microfluid. Nanofluid.*, 2016, **20**, 54.
41 I. Vlassiouk, S. Smirnov and Z. S. Siwy, *Nano Lett.*, 2008, **8**, 1978–1985.
42 B. J. Kirby, *Micro- and nanoscale fluid mechanics*, Cambridge University Press, 2010.
43 A. T. Conlisk, *Essentials of Micro-and Nanofluidics*, Cambridge University Press, 2012.
44 F. H. J. van der Heyden, D. Stein, K. Besteman, S. G. Lemay and C. Dekker, *Phys. Rev. Lett.*, 2006, **96**, 224502.
45 C. Zhong, Y. Deng, W. Hu, J. Qiao, L. Zhang and J. Zhang, *Chem. Soc. Rev.*, 2015, **44**, 7484–7539.
46 D. Gillespie, *Microfluid. Nanofluid.*, 2015, **15**, 717–738.
47 J. Hoffman and D. Gillespie, *Langmuir*, 2013, **29**, 1303–1317.
48 S. Joseph and N. R. Aluru, *Langmuir*, 2006, **22**, 9041–9051.
49 J. A. Rard and D. G. Miller, *J. Chem. Eng. Data*, 1980, **25**, 211–215.
50 R. Qiao and N. Aluru, *Langmuir*, 2005, **21**, 8972–8977.
51 R. Qiao, J. G. Georgiadis and N. R. Aluru, *Nano Lett.*, 2006, **6**, 995–999.
52 S. N. Bush, J. S. Ken and C. R. Martin, *ACS Nano*, 2022, **16**, 8338–8346.
53 K. Lin, C.-Y. Lin, J. W. Polster, Y. Chen and Z. S. Siwy, *J. Am. Chem. Soc.*, 2020, **142**, 2925–2934.
54 J. Ma, Z. Zhang, X. Gu, K. Li, D. Li and Y. Chen, *J. Phys. Chem. C*, 2022, **126**, 14661–14668.
55 A. Paul and N. R. Aluru, *Phys. Rev. E*, 2024, 025105.
56 R. Qiao and N. R. Aluru, *Colloids Surf., A*, 2005, **267**, 103–109.
57 A. Alizadeh, W.-L. Hsu, M. Wang and H. Daiguji, *Electrophoresis*, 2021, **42**, 834–868.
58 Y. Green, *ACS Omega*, 2022, **7**, 36150–36156.